Current Biology

Stem cell niche organisation in the Drosophila ovary requires the ECM component Perlecan

--Manuscript Draft--

Manuscript Number:	CURRENT-BIOLOGY-D-20-01366R2
Full Title:	Stem cell niche organisation in the Drosophila ovary requires the ECM component Perlecan
Article Type:	Report
Corresponding Author:	Acaimo Gonzalez-Reyes, Ph.D. Spanish National Research Council-CSIC Sevilla, SPAIN
First Author:	Alfonsa Díaz-Torres
Order of Authors:	Alfonsa Díaz-Torres
	Alicia E. Rosales-Nieves
	John R. Pearson
	Carmen Santa-Cruz Mateos
	Miriam Marín-Menguiano
	Owen J. Marshall
	Andrea H. Brand
	Acaimo Gonzalez-Reyes, Ph.D.
Abstract:	Summary Stem cells reside in specialised microenvironments or niches that balance stem cell proliferation and differentiation [1, 2]. The extracellular matrix (ECM) is an essential component of most niches, as it controls niche homeostasis, provides physical support and conveys extracellular signals [3-11]. Basement membranes (BMs) are thin ECM sheets constituted mainly by Laminins, Perlecan, Collagen IV and Entactin/Nidogen and that surround epithelia and other tissues [12]. Perlecans are secreted proteoglycans that interact with ECM proteins, ligands, receptors and growth factors such as FGF, PDGF, VEGF, Hedgehog and Wingless, [13-18]. Thus, Perlecans have structural and signalling functions through the binding, storage or sequestering of specific ligands. We have used the Drosophila ovary to assess the importance of Perlecan in the functioning of a stem cell niche. Ovarioles in the adult ovary are enveloped by an ECM sheath and possess a tapered structure at their anterior apex termed the germarium. The anterior tip of the germarium hosts the germline niche, where two to four germline stem cells (GSCs) reside together with few somatic cells: terminal filament (TF) cells, cap cells (CpCs) and escort cells (ECs) [19]. We report that niche architecture in the developing gonad requires trol, that niche cells secrete an isoform-specific, Perlecan-rich interstitial matrix and that D E-cadherin-dependent stem cell-niche adhesion necessitates trol . Hence, we provide evidence to support a structural role for Perlecan in germline niche establishment during larval stages and in the maintenance of a normal pool of stem cells in the adult niche.

Submission date: 15-ene.-21

Stem cell niche organisation in the *Drosophila* ovary requires the ECM component Perlecan

Alfonsa Díaz-Torres[1, 4], Alicia E. Rosales-Nieves[1, 5], John R. Pearson[1, 6], Carmen Santa-Cruz Mateos[1], Miriam Marín-Menguiano[1], Owen J. Marshall[2], Andrea H. Brand[3] and Acaimo González-Reyes[1, 7, *, #]

[1]Centro Andaluz de Biología del Desarrollo,
CSIC/Universidad Pablo de Olavide/JA,
Carretera de Utrera km 1,
41013 Sevilla, Spain

[2]The Gurdon Institute and Department of Physiology, Development and Neuroscience,
University of Cambridge,
Downing Street, Cambridge CB2 1QN, UK
and Menzies Institute for Medical Research
University of Tasmania, 17 Liverpool St, Hobart 7000, Australia

[3]The Gurdon Institute and Department of Physiology, Development and Neuroscience,
University of Cambridge,
Downing Street, Cambridge CB2 1QN, UK

[4]Current address: Microscopy Unit,
Centro Nacional de Investigaciones Cardiovasculares (CNIC),
28029 Madrid, Spain

[5]Current address: Instituto de Biomedicina de Sevilla (IBiS)
Hospital Universitario Virgen del Rocío/CSIC/Universidad de Sevilla
41011 Seville, Spain

[6]Current address: Centro Andaluz de Nanomedicina y Biotecnología (BIONAND),
C/ Severo Ochoa 35, Parque Tecnológico de Andalucía,
29590 Campanillas (Málaga), Spain

[7]Lead contact

*Correspondence to: AG-R (e-mail: agonrey@upo.es; phone: +34-954 348672; fax: +34-954 349376)

[#]AG-R dedicates this work to Professor José Luis Gómez-Skarmeta, an inspirational colleague and friend, on the occasion of his untimely demise.

SUMMARY

Stem cells reside in specialised microenvironments or niches that balance stem cell proliferation and differentiation [1, 2]. The extracellular matrix (ECM) is an essential component of most niches, as it controls niche homeostasis, provides physical support and conveys extracellular signals [3-11]. Basement membranes (BMs) are thin ECM sheets constituted mainly by Laminins, Perlecan, Collagen IV and Entactin/Nidogen and that surround epithelia and other tissues [12]. Perlecans are secreted proteoglycans that interact with ECM proteins, ligands, receptors and growth factors such as FGF, PDGF, VEGF, Hedgehog and Wingless, [13-18]. Thus, Perlecans have structural and signalling functions through the binding, storage or sequestering of specific ligands. We have used the *Drosophila* ovary to assess the importance of Perlecan in the functioning of a stem cell niche. Ovarioles in the adult ovary are enveloped by an ECM sheath and possess a tapered structure at their anterior apex termed the germarium. The anterior tip of the germarium hosts the germline niche, where two to four germline stem cells (GSCs) reside together with few somatic cells: terminal filament (TF) cells, cap cells (CpCs) and escort cells (ECs) [19]. We report that niche architecture in the developing gonad requires *trol,* that niche cells secrete an isoform-specific, Perlecan-rich interstitial matrix and that *D*E-cadherin-dependent stem cell-niche adhesion necessitates *trol*. Hence, we provide evidence to support a structural role for Perlecan in germline niche establishment during larval stages and in the maintenance of a normal pool of stem cells in the adult niche.

RESULTS AND DISCUSSION

CpCs organise into a 6-8 cell rosette positioned at the base of the TF. Both cell types are connected by the “transition cell” [20]. TF cells and CpCs can be distinguished from their characteristic shape, from their Engrailed (En) expression and from their high Lamin C contents. GSCs are anchored to the adjacent CpC rosette by adherens junctions and this adhesion prevents GSC loss from the niche [21] (Figure 1A, A’).

The *Drosophila* ovarian niche possesses a specialised extracellular matrix

We determined the pattern of expression of Perlecan in relation to Collagen IV, Laminin β and Nidogen in the ovarian niche and early egg chambers (Figure 1B-F). As previously reported [11], Collagen IV::GFP (ColIV::GFP) [22, 23] is strongly expressed in the matrix surrounding the niche and a discrete signal is detected in the interstitial space between TFCs and CpCs (Figure 1B). Laminin β and Nidogen display similar patterns of expression except that their interstitial signal is even less conspicuous than that of ColIV::GFP (Figure 1C, D). They all are expressed in the BM of young egg chambers.

The *terribly reduced optic lobes (trol)* gene, which encodes the Perlecan proteoglycans in *Drosophila* [17, 18, 24, 25], is predicted to produce 23 different isoforms transcribed from three different promoters, giving rise to one short isoform (RBB), one intermediate (RAK) and 21 long isoforms, two of which are truncated at their 3' ends (*trol-RAG* and *trol-RAX*). Except *trol-RAG* and *trol-RAX*, the rest of the isoforms contain all of the conserved domains found in *Drosophila* Perlecan (domains II to V of the human homologue; Figure S1A). To define Perlecan distribution in the niche and in early oogenesis, we used a *trol::GFP* line in which only long isoforms are targeted. Similarly to Laminin, ColIV::GFP and Nidogen, Perlecan::GFP accumulates in the BM surrounding the ovariole without detectable expression between niche cells (Figure 1E). A Perlecan antibody that recognises domain V of the protein localised to the BM around the niche and from S3 onwards, whereas in S1-S2 egg chambers it strongly accumulates in vesicle-like dots inside the follicle cells [26]. In clear contrast to the distribution of Perlecan::GFP, Perlecan antibody localised strongly around TF cells, in CpC-CpC boundaries and in CpC-GSC contacts, albeit less pronouncedly in the latter. This suggests the accumulation of a specialised interstitial matrix around TF and cap cells, an idea further confirmed by the presence of deposits of electron-dense material in the intercellular spaces between CpCs and the CpC-GSC boundaries in transmission electron micrographs (Figure 1F-H). We conclude that the short and/or the intermediate Perlecan isoforms accumulate specifically in the interstitial matrix of the GSC niche, while the long isoforms are incorporated mainly into the BM.

The male GSC niche exhibits a number of similarities with its female equivalent, including a cluster of highly packed hub cells that resemble cap cells as they act as a signalling centre [27]. Male GSCs surround the hub cells and are flanked by somatic cyst stem cells. As

in the case of the ovariole, the whole structure is surrounded by BM and a muscle sheath (reviewed in [28]). However, in spite of these similarities, hub cells were not surrounded by a deposition of Perlecan protein, even though Perlecan accumulated in the basement membrane and the muscle sheath of the apical end of the testis (Figure S1B, C).

Gene expression profiling identifies niche-specific *trol* isoforms

Next, we used Targeted DamID (TaDa) to test whether the presumptive niche-specific localisation of Perlecan variants corresponded with differential expression of *trol* isoforms. TaDa utilises the Gal4/UAS system to express Dam-Pol II, a fusion of the Dam methylase and the RNA polymerase II core subunit RpII215, to define cell-type specific transcriptomes [29]. In combination with *tub-Gal80^{ts}*, we first expressed Dam-Pol II in adult niche cells using *en-Gal4* and *bab1-Gal4*. As a positive control for *trol* isoform trnascription we expressed Dam-Pol II in most of the somatic cells of the ovary with *tj-Gal4* (Figure 2A) [20, 30]. To control for non-specific methylation, we expressed the Dam methylase alone using the same drivers. Due to the reduced numbers of target cells for the *en-* and *bab1-Gal4* drivers compared to *tj-Gal4*, we combined their profiles to define those genes expressed in niche cells. Only genes with an FDR (False discovery rate of enriched Pol II occupancy) <0.01 were considered. As a positive control, we first checked that the expression of the ubiquitously-expressed gene *Act5c* was detected in all datasets (Figure S1D).

We identified 5032 genes, 1614 specific to the *tj*-positive cells and 877 exclusive to the *en+bab1* sets and that may represent niche-specific genes expressed in TF cells and likely enriched in cap cells (Data S1 and Figure 2A). Surprisingly, niche genes such as *dpp*, *gbb*, *upd* and *hh* [19, 31-35] were not among the identified genes. It is conceivable that during the initial procedure of DNA extraction DNA shearing could not be completely avoided due to the high cell numbers in the ovary, resulting in higher levels of non-specific signal. Hence, low-level expressed genes could be under-represented and may fall below the implemented FDR<0.01 threshold. Nevertheless, we identified several niche genes including *hopscotch*, *shotgun* and several of the *innexin* genes [21, 36, 37], indicating that our approach, albeit with some limitations, is a valid strategy for defining the niche transcriptome.

We used Pol II occupancy profile peaks and direct comparison with the predicted transcription start (TSS) and transcription end (TES) sites of the different isoforms to define the *trol* variants transcribed in niche cells. *tj-Gal4*-expressing cells utilise all three TSSs and both TESs, indicating that these cells actively transcribed all four isoform types (Figure 2B, C; Figure S1A). In *en-Gal4 + bab1-Gal4* cells, which did not seem to express the intermediate RAK isoform nor the RAG and RAX truncated long isoforms, the promoters giving rise to long and the short (RBB) isoforms were active. Since TF cells express Perlecan::GFP and since CpCs accumulate Perlecan but not Perlecan::GFP, our results indicate that CpCs mainly express *trol-RBB*, the short isoform. While we cannot exclude that post-transcriptional modifications of the Perlecan protein affect its stability and/or localisation and, hence, that the accumulation of Perlecan or Perlecan:GFP could occur away from the producing cells, we find this unlikely, since CpCs lacking the *trol* gene do not accumulate Perlecan (see below), which suggests a very limited diffusion of the protein from the producing cap cells.

trol activity is required for niche organisation

To test if Perlecan had a role in niche architecture, we used RNA interference to decrease *trol* function. TFs and CpCs from *bab1-Gal4, UAS-trol RNAi* (*bab1>trol RNAi*) females grown at 25^{o}C showed a ~7-fold reduction in Perlecan proteins when compared to controls (Figure 3A, B). These *bab1>trol RNAi* germaria displayed a number of mutant phenotypes. First, the number of CpCs in experimental rosettes was lower than in controls (7.1±1.21 CpCs in controls; 6±1.54 in *bab1>trol-RNAi*; Figure 3C). Second, in 22% of experimental germaria we observed abnormal CpC rosettes in which individual, or groups of, Lamin C-positive cells were displaced from the base of the TF. These displaced CpCs also expressed Engrailed, another cap cell marker (Figure 3A, D; Video S1). This phenotype was found even in germaria from freshly eclosed females. Third, the number of GSCs/niche was also significantly reduced in *bab1>trol RNAi* flies (2.70±0.56 in controls; 2.37±0.71 in experimental ones; Figure 3E). Furthermore, 10% of *bab1>trol RNAi* germaria analysed contained 0 or 1 GSC/niche, whereas all of the control niches hosted ≥2 GSCs (Figure 3E). These results confirm that *trol* is required to maintain GSC niche integrity and to preserve a normal pool of stem cells within it.

Next, we generated *trol* null CpCs during larval and pupal stages, which is when CpC precursors proliferate and mitotic clones can be induced. We observed that *trol*$^{-}$ CpCs (recognised by the round shape of their nuclei, the loss of GFP signal and by their expression of Lamin C) could be found displaced from their normal location at the base of the TF in 7% of mosaic germaria (Figure 3F, G; Figure S2A; Video S2). A detailed analysis of the aberrant niches confirmed that only those germaria containing ≥3 mutant CpCs showed the CpC displacement phenotype (50% of niches with ≥3 mutant CpCs; Figure 3F'). Mutant cells — even those still located in the rosette — failed to accumulate Perlecan, indicating that CpCs autonomously produced the surrounding Perlecan (Figure S2B, planes z3 and z4). Thus, our results strongly suggest that Perlecan protein is required for the proper establishment and/or maintenance of the CpC rosette and, as a consequence, for hosting a normal GSC pool within the niche. The fact that at least three *trol*$^{-}$ CpCs are needed to observe the displacement phenotype suggests that Perlecan secreted from neighbouring *trol*$^{+}$ CpCs can rescue the loss of *trol* activity in individual CpCs. TF cells mutant for *trol* also display reduced Perlecan levels, indicating that, at least partially, TF cells secrete Perlecan (Figure S2C, D). Finally, we generated *trol::GFP;; bab1-Gal4/UAS-sh:GFP* (*trol::GFP;; bab1>GFP RNAi*) flies and grew them at 25 ^{o}C to deplete the developing gonads and the adult niches of long Perlecan isoforms. 1-week-old control germaria showed alterations in the organisation of niche cells in 13,8% of the samples, while experimental germaria displayed aberrant niches containing displaced CpCs, individual or in clusters, in 25,6% of the cases (Figure S2E).

trol is required for niche establishment during larval stages

We then studied if *trol* function was required during niche formation in third instar larvae/early pupae. Larval gonads can be divided into three regions: an anterior one where TF cells and CpC precursors are located; a central region, which houses the primordial germ cells (PGCs) intermingled with their somatic cell neighbours (ISCs); and a posterior region [38]. ISCs and the future CpCs express the Traffic-jam protein [39] (Figure 4). At late third-instar larval stage, TF cells differentiate and arrange into the separate stalks that will constitute the ovarioles' anterior tip. TFs appear in a morphogenetic wave from medial to lateral positions across the gonad until early pupal development [39, 40]. At the larval-to-pupal transition,

some of the somatic cells juxtaposed with the TFs differentiate into CpCs or ECs, primordial germ cells (PGCs) located next to the newly formed CpCs convert into GSCs, and the niche becomes a functional unit that hosts on average 2-4 GSCs (Figure 4A).

Perlecan localisation in developing gonads is consistent with a role during niche formation. At mid- and late-third instar larval gonads (ML3 and LL3) Perlecan is found lining the gonad periphery, at the interface with the fat body, but it is also detectable internally, within the gonadal cells. We observed regions of strong localisation between the anterior somatic cells and in the area where the PGCs gather together. Importantly for our studies, Perlecan accumulation was detected between the developing niche and the PGCs, delimiting both regions in ML3 (Figure 4B). We found that this interstitial accumulation of Perlecan increased over time and was abundantly distributed in the PGC region and in patches in between somatic cells at LL3. Perlecan::GFP showed a similar distribution (Figure 4C and Video S3).

To assess the importance of Perlecan for niche establishment in larvae we removed Perlecan from large regions of the gonad using RNA interference. First, we used *traffic jam-Gal4, UAS-trol RNAi* (*tj>trol RNAi*) to knock down Perlecan from CpCs and ISCs. Perlecan was hardly detectable in the PGC region or in the boundary between the forming niche and the rest of the gonad of *tj>trol RNAi* larvae, even though Perlecan still surrounded the external perimeter of the gonad (Figure S3A). We detected no obvious alterations to ISC number or arrangement nor to the organisation of the presumptive CpCs abutting the TFs (as determined by Tj-positive staining). These results show that the *trol* RNAi approach is an effective tool to reduce significantly Perlecan amounts in developing gonads and that a large proportion of the Perlecan found inside the gonad is secreted by *tj*-positive ISCs and CpCs. We then reduced Perlecan from most somatic cells of the gonad utilising the *bab1-Gal4* line. LL3 *bab1>trol RNAi* larvae grown at 25^{o}C (the same conditions that had previously given the CpC displacement phenotype in adult flies), possessed gonads without any obvious defects in the organisation of TF and ISCs when compared to control ones (Figure 4D, E). However, the resolution of our analysis may be compromised by the large cellular rearrangements that take place in larval gonads.

To determine if the displaced CpCs found in adult *bab1>trol RNAi* niches or in mosaic germaria resulted from reduced Perlecan amounts during larval/pupal gonadal development or from the loss of *trol* function in the adult, we first looked at germaria from freshly eclosed (0 to 24h-old) *bab1>trol RNAi* females grown at 25^{o}C. We found displaced CpCs in 18.3% of experimental samples compared to 0% in control ones (Figure 4 F, G). Next, we utilised the *tubulin-Gal80^{ts}* system to reduce *trol* activity only in adult niches. On this occasion, we also co-expressed the *Dicer-2* gene to enhance the RNAi phenotype. Thus, we raised *bab1-Gal4, tubulin-Gal80^{ts}, UAS-trol RNAi, UAS-Dicer-2* (*bab1^{ts}>trol RNAi + Dicer-2*) flies at 18^{o}C till eclosion and then placed the adults at 29^{o}C for 7 days to induce *trol RNAi* expression in the adult GSC niche. With this approach, Perlecan levels were reduced 7.5 times in experimental germaria compared to controls (Figure S3B). Nevertheless, we failed to observe CpC displacement in *bab1^{ts}>trol RNAi + Dicer-2* germaria (n= 30). Our results demonstrate that maintaining CpC rosette organisation in the adult does not require high levels of Perlecan protein and they strongly suggest that *trol* is needed during larval/pupal development for correct organisation of the adult GSC niche.

trol activity regulates _D_E-cadherin levels in CpCs

Drosophila Epithelial (*D*E)-cadherin-mediated cell adhesion plays an important role during the initial stages of gonad formation in the embryo and in larval stages. In the adult, *D*E-cadherin mediates CpC-GSC and EC-GSC attachment and prevents stem cell loss from the niche [21, 41-43]. Considering the aberrant architecture of Perlecan mutant niches, we determined if removal of *trol* function affected *D*E-cadherin localisation. We quantified *D*E-cadherin levels at CpC-CpC and CpC-GSC boundaries in mosaic germaria containing control and *trol^{-}* CpCs. Upon close examination of 69 boundaries from 21 germaria, we found that loss of *trol* function decreased membrane *D*E-cadherin in both, CpC-CpC and CpC-GSC boundaries (68.8±17.5 average fluorescence intensity in *trol^{+}/trol^{+}* CpC boundaries and 46.4±14.8 in *trol^{+}/trol^{-}*; 72.7±18.9 in *trol^{+}* CpC/GSC boundaries and 45.4±17.2 in *trol^{-}* CpC/GSC; Figure 4H, I). Analysis of mosaic LL3 gonads indicated that mutant larval TF and CpCs also displayed lower *D*E-cadherin levels compared to paired controls (21.2±6.1 in controls; 13.0±4.9 in experimental ones; Figure S3C, D). Since *trol* was required in LL3 gonads and in the adult

niche for proper *D*E-cadherin accumulation, we surmised that the CpC displacement phenotype was a consequence of impaired *D*E-cadherin-mediated adhesion between the mutant CpCs and other niche cells. This impaired adhesion may also explain, at least partially, the slight reduction in GSC numbers in *trol*-deficient niches (Figure 3E). To test this, we removed one copy of *shotgun,* the gene encoding for *D*E-cadherin [44] and looked at *bab1>trol RNAi* adult niches. We found that *+/+; bab1>trol RNAi* and *shotgun/+; bab1>trol RNAi* females displayed similar GSC numbers. However, the former showed milder CpC displacement phenotypes compared to the latter (14.3% *vs* 19.5%, respectively; Figure S3E, F). Our results thus provide a direct link between loss of *trol* activity and reduced levels of a cell-cell adhesion molecule.

The finding that CpCs produce mainly the short *trol-RBB* isoform indicates a regional distribution of Perlecan variants in the niche. In addition, our mosaic analysis strongly suggests that CpCs cell-autonomously deposit interstitial Perlecan. This is in contrast to other instances in which ECM components are secreted non-autonomously by other cell types or even tissues [22, 45, 46]. The reason(s) for this short-range secretion could be due to a local characteristic of the interstitial matrix around CpCs that limits the range of Perlecan diffusion or it may lie in the RBB-encoded Perlecan having different biochemical properties *versus* the longer isoforms. In fact, *trol-RBB* contains one small, 78 amino acid-long exon in which 12 serine and tyrosine residues are predicted targets for O-glycosylation. This heavily-glycosylated exon — present only in the short (RBB), the intermediate (RAK, but it is not expressed in the niche) and the long RBA and RAS (Figure S1A) — may confer the RBB protein biochemical properties that could explain its compartmentalised localisation in the niche.

Stem cells are capable of self-renewing or to produce tissue-specific cell types. A number of factors control their behaviour, including signals from nearby niche cells or the surrounding ECM [4]. Our work identifies a specialised matrix secreted by cap cells, rich in a specific Perlecan isoform and that is functionally relevant. This novel function of Perlecan in the formation of a proper stem cell niche may be of general importance, given the widespread presence of ECM components associated with stem cells and their niches [5, 47].

ACKNOWLEDGMENTS

We thank the BDSC and the VDRC for fly stocks and the DSHB (University of Iowa) for antibodies. TEM analysis was performed at the CIC, University of Granada. This work was funded by the Spanish State Research Agency (MCUI/AEI, http://www.ciencia.gob.es/; Grant numbers BFU2015-65372-P, PGC2018-097115-B-I00 and MDM-2016-0687 to AG-R) and by the European Regional Development Fund (http://ec.europa.eu/regional_policy/en/funding/erdf/). AHB was supported by the Royal Society Darwin Trust Research Professorship and Wellcome Trust Senior Investigator Award 103792. AHB acknowledges core funding to the Gurdon Institute from the Wellcome Trust (092096) and CRUK (C6946/A14492). OJM was supported by an EMBO long-term fellowship (ALTF 423-2011).

AUTHOR CONTRIBUTIONS

AD-T, AR-N, JRP and AG-R conceived and designed research; AD-T, AR-N, JRP, CS-CM, MM-M and OJM performed research; AD-T, OJM, AHB and AG-R analysed data. JRP and AG-R wrote the paper.

DECLARATION OF INTERESTS

The authors declare no competing interests.

FIGURE LEGENDS

Figure 1: **Distribution of basement membrane components in control ovarioles. (A, A')** Scheme of a control ovariole showing the germarium and the GSCs within, the cellular organisation of the follicular epithelium, the posteriorly placed oocyte and the surrounding basement membrane (BM). Egg chambers of different stages (S) are shown. The magnification in (A') depicts GSC niche components. **(B, B')** Collagen IV distribution, as shown by the distribution of the fusion protein Col IV::GFP, encoded by the *viking::GFP* (*vkg::GFP*) gene. **(C, C')** Laminin ß expression pattern as shown with an anti-Laminin ß antibody. **(D, D')** Nidogen expression, detected with an anti-Nidogen antibody. **(E, E')** Localisation of the Perlecan::GFP fusion protein, encoded by *trol::GFP*. **(F, F')** Perlecan accumulation, as

visualised with an anti-Perlecan antibody. Note that the Perlecan::GFP protein trap clearly accumulates in the BM, while the anti-Perlecan antibody shows strong staining in TFcells and CpCs, and in the BM of S3 and later egg chambers. The Perlecan staining is so much stronger in the interstitial matrix between niche cells that the confocal gain has to be reduced to avoid saturating the image. Thus, the weaker anti-Perlecan signal in the niche BM often goes undetected. **(G-G'')** Perlecan accumulates in the TF and CpC rosette, which are labelled with Lamin C. **(H)** Transmission electron micrograph of a control niche. CpCs, ECs and GSCs are pseudo-coloured. Note the electron-dense material that surrounds the entire germarium tip and that is also found enclosing the CpCs. Empty arrowheads point to the interstitial matrix present in the niche. Panels B-F correspond to different z-sections stitched together in a single plane. Scale bar (B-F) = 50µm. Scale bar (G) = 15µm. See also Figure S1.

Figure 2: Transcription of *trol* isoforms in different somatic cell types of the adult ovary. (A) Workflow for the TaDa analysis. The Dam-Pol II fusion protein was expressed in TF cells, CpCs and ECs using the *engrailed-Gal4* and *bric-a-brac 1-Gal4* (*en-Gal4 + bab1-Gal4*) lines. The *traffic jam-Gal4* (*tj-Gal4*) line is expressed in most of the somatic cells of the ovary except the TF. **(B)** The twenty-three isoforms encoded by the *trol* gene can be grouped into four types: one short isoform (*trol-RBB*), an intermediate isoform (*trol-RAK*), two long isoforms with truncated 3' ends (*trol-RAG* and *trol-RAX*) and nineteen long versions. Of the latter groups, only *trol-RAG* and the long isoform *trol-RAT* are shown. Compared to its human orthologue, *Drosophila* Perlecan proteins contain domains II-V but lack Domain I. The insertion point of the artificial GFP-encoding exon, the translation initiation codons (arrows) and the translational stop codons (solid black circles) are shown. **(C)** Differential Pol II occupancy of *trol* in *tj*-positive cells (*tj-Gal4*) or in niche cells (*en-Gal4 + bab1-Gal4*) of the adult ovary. Scale bars represent log2 ratio change between Dam-Pol II and Dam (reference) samples. The data are scaled so that the Pol II occupancy between the two different cell types should be equivalent. *tj-Gal4* cells express all four types of isoforms and use the three TSSs and both TESs. *en-Gal4 + bab1-Gal4* cells transcribe neither the intermediate *trol-RAK* nor the long, truncated versions *trol-RAG* and *trol-RAX.* (See Figure S1A for a representation of all *trol* isoforms). The peaks are larger at the beginning of transcription due to the longer duration of

the transcription initiation phase, which increases the chance of Pol II binding to the TSS regions and thus the possibility of being identified in the TaDa analysis. TSS: Transcriptional Start Sites; TES: Transcriptional End Sites. See also Data S1 and Figure S1.

Figure 3: Loss of *trol* activity induces cap cell displacement. (A) Immunodetection of Perlecan, Lamin C and Engrailed in control and *bab1>trol RNAi* germaria. *bab1>trol RNAi* germaria show reduced Perlecan levels and displaced CpCs (arrows). Images are maximum projections of two sections along the Z-axis. **(B)** Quantification of the Perlecan immunofluorescence signal in control and *bab1>trol RNAi* germaria. **(C)** Graph displaying the number of CpCs per rosette in niches of the above genotypes. **(D)** Percentage of control and experimental germaria showing displaced CpCs. **(E)** Quantification of the number of GSCs per niche and distribution of germaria containing 0-1 or 2-4 GSCs in control and experimental germaria. **(F)** Graph representing the analysis of 73 mosaic germaria containing 1 to 4 *trol* mutant CpC. 6.7% of mosaic niches show displaced CpCs. **(F')** Niches with 1-2 mutant CpCs do not show displaced cells while ~50% of those containing 3-4 *trol*$^{-}$ CpCs display the phenotype. The appearance of displaced CpCs thus requires at least three *trol*$^{-}$ CpCs in a given niche. **(G)** Single z-section of a mosaic germarium containing a displaced *trol* mutant CpC (see Figure S2 and Video S2 for further details). (A-E) Germaria from flies grown at 25^{o}C. Arrows: displaced *trol*$^{-}$ CpCs; arrowhead: mutant CpC in the rosette. Clones were induced using the *bab1-Gal4/UASt-flp* system. P values of two-tailed, unpaired t-tests considered statistically significant between control and experimental samples are indicated (*: P≤0.05, **: P≤0.005, ***: P≤0.0005). Numbers in bars refer to number of germaria analysed. Scale bars = 10µm. See also Figure S2 and Videos S1 and S2.

Figure 4: Perlecan expression in the larval gonad. (A) Scheme of a mid-third instar larval (ML3) gonad showing the medial-to-lateral morphogenetic wave of terminal filament (TF) formation, the arrangement of the newly-determined cap cells and the organisation of the primordial germ cells (PGCs) and their associated intermingled somatic cells (ISCs). **(B)** Z-projection of an ML3 gonad stained to visualise Perlecan and Traffic jam (to label future CpCs

and ISCs). Notice the conspicuous Perlecan accumulation in the boundary region between the TF cells and the PGCs/ISCs. **(C)** Z-projection of 1.5µm of a late-third instar larval (LL3) gonad stained to visualise Perlecan, Traffic jam and Engrailed (to label TF cells). Empty arrowheads point to accumulations of Perlecan in the forming GSC niches. LL3 gonads are found in larvae of 118-128 hours of age after egg laying. **(D)** Single plane of a control LL3 gonad stained to visualise Perlecan, Traffic jam, DNA and Hts (to label spectrosomes/fusomes and the outline of most cells). The Perlecan signal in (D) appears weaker than in (C) because the latter corresponds to the projection of several z-planes. **(E)** Single plane of an experimental *bab1>trol RNAi* LL3 gonad stained to visualise Perlecan, Traffic jam, DNA and Hts. Notice the obvious decrease in Perlecan staining inside the *trol* RNAi gonad. **(F, G)** Control (F) and *bab1>trol RNAi* experimental (G) germaria from freshly eclosed females stained to detect Perlecan, Lamin-C and DNA. Images in (F, G) are z-projections of 3.15µm of the samples; inset in (G) corresponds to a displaced CpC in a different focal plane. See Video S4 for a complete view of the experimental germarium. **(H)** Z-projections of a mosaic germarium containing $trol^{-}$ CpCs stained to visualise *D*E-cadherin (*D*E-cad), GFP and DNA. **(I)** Quantification of *D*E-cadherin levels at $trol^{+}/trol^{+}$ or $trol^{+}/trol^{-}$ paired CpC boundaries, and at $trol^{+}$ CpC/$trol^{+}$ GSC or $trol^{-}$ CpC/$trol^{+}$ paired GSC surfaces. $trol^{-}$ CpCs localise significantly lower *D*E-cadherin amounts at their surfaces facing CpCs or GSCs than $trol^{+}$ CpCs. Empty arrowheads: control CpCs in the rosette; solid arrowheads: mutant CpCs in the rosette; asterisks: GSCs. P values of two-tailed, paired t-tests considered statistically significant between control and experimental samples are indicated (**: P≤0.005, ***: P≤0.0005). The mean (cross) and median (line across box) for each of the samples are shown. We quantified 10 $trol^{+}/trol^{+}$ and 11 $trol^{+}/trol^{-}$ CpC boundaries from 8 germaria; and 28 $trol^{+}$ CpC/GSC and 20 $trol^{-}$ CpC/GSC boundaries from 13 germaria. Clones were induced using the *bab1-Gal4/UASt-flp* system. Arrow: displaced CpC. Scale bars = 10µm. See also Figure S3 and Videos S3 and S4.

STAR METHODS

RESOURCE AVAILABILITY

Lead Contact

Further information and requests for resources and reagents should be directed to and will be fulfilled by the Lead Contact, Acaimo González-Reyes (agonrey@upo.es).

Materials Availability

Fly lines generated in this study and the anti-Perlecan antibody are available without restrictions from the Lead Contact.

Data and Code Availability

DamID sequencing data are available from the GEO website (https://www.ncbi.nlm.nih.gov/geo/; accession number GSE164866).

EXPERIMENTAL MODEL AND SUBJECT DETAILS

Fruit flies *D. melanogaster* were reared on standard wheat flour-agar medium or on the richer Nutri-Fly™ "German Food" Sick Fly Formulation (Genesee Scientific). Flies were grown at 25^{o}C with relative humidity of approx. 50% and a 12h dark/12h light cycle, unless otherwise noted. For strain details see the Key Resource Table.

METHOD DETAILS

Fly stocks

The *traffic jam-Gal4* driver *(tj-Gal4*) is expressed in most of the somatic cells of the ovary, including the epithelial sheath [20, 30, 48]. *bric-a-brac 1-Gal4* (*bab1-Gal4*) is expressed at higher levels in TFCs and CpCs, and weakly in ECs and in few germarial follicle cells [49]. *engrailed-Gal4* (*en-Gal4*) is expressed in TFCs and CpCs [50].

For loss-of-function experiments, we either used RNA interference or induced somatic clones utilising the FRT/FLP technique. The RNAi knockdown was performed using the Gal4-UAS system. To knock-down *trol* RNA levels, flies of the appropriate genotype were either grown and kept at 25°C or, when harbouring the *tub-Gal80^{ts}* construct, grown at 18°C and shifted from 18°C to 29°C for one week upon hatching and prior to dissection. The RNAi construct used should target all known *trol* isoforms (Figure S1A). To induce somatic clones with the FRT/FLP technique [51], we generated either *trol^{null}* FRT-101/*hs-flp12 ubi-nlsGFP* FRT-

101 or *trol*^{null} FRT-101/*hs-flp12 ubi-nlsGFP* FRT-101;; *bab1-Gal4 UASt-flp*/TM2 females. In the former genotype, recombination between the FRT-101 sites was induced by the activation of the *hs-flp* transgene after transferring adult females or larvae to 37°C for 1 hour. In the latter, recombination was achieved by the *bab1-Gal4*-mediated expression of *UASt-flp* or, when indicated, by both, *bab1-Gal4/UASt-flp* and by heat-shock. Mutant clones were marked by the absence of GFP. *trol*^{null} is a deletion of the entire gene that eliminates all known *trol* isoforms [18]. In RNAi experiments, *bab1-Gal4* or *tj-Gal4* were combined with the corresponding *UASt-RNAi* line.

Experimental genotypes

Figure 1

(B) *w*; *viking::GFP*

(C, D, F, G, H) *y w*

(E) *w; trol::GFP*

Figures 3

(A-E) control: *w, UASt-trol RNAi/+;; TM6B/+*

bab1>trol RNAi: w, UASt-trol RNAi/+;; bab1-Gal4/+

(F, G) *w, trol*^{null} *FRT-101/y w, hs-FLP12 pUbi-nls GFP FRT-101; bab1-Gal4, UASt-FLP/+*

Figure 4

(B, C) *y w*

(D-G) control*: w, UASt-trol RNAi/+;; TM6B/+*

bab1>trol RNAi: w, UASt-trol RNAi/+;; bab1-Gal4/+

(H) *w, trol*^{null} *FRT-101/y w, hs-FLP12 pUbi-nls GFP FRT-101; bab1-Gal4, UASt-FLP/+*

Figure S1

(C) *y w*

Figure S2

(A-D) *w, trol*^{null} *FRT-101/y w, hs-flp12 pUbi-nls GFP FRT-101; bab1-Gal4, UASt-FLP/+*

(E) control: *trol::GFP;; UAS-sh:GFP/TM2*

trol::GFP;; bab1>GFP RNAi: trol::GFP;; bab1-Gal4/UAS-sh:GFP

Figure S3

(A) *tj>trol RNAi: w, UASt-trol RNAi/+; tj-Gal4/+*

(B) control: *w, UASt-trol RNAi/+;; TM6B/+*

bab1^{ts}>trol RNAi+Dicer-2: w, UASt-trol RNAi/+; tub-Gal80^{ts}/+; bab1-Gal4/UAS-Dicer-2

(C) *w, trol^{null} FRT-101/y w, hs-flp12 pUbi-nls GFP FRT-101*

(E, F) control +/+: *w, UASt-trol RNAi/+; Gla/+; TM6B/+*

control *shg*/+: *w, UASt-trol RNAi/+; shg^{1}/+; TM6B/+*

bab1>trol RNAi: w, UASt-trol RNAi/+; Gla/+; bab1-Gal4/+

shg/+; bab1>trol RNAi: w, UASt-trol RNAi/+; shg^{1}/+; bab1-Gal4/+

Video S1

bab1>trol RNAi: w, UASt-trol RNAi/+;; bab1-Gal4/+

Video S2

w, trol^{null} FRT-101/y w, hs-FLP12 pUbi-nls GFP FRT-101; bab1-Gal4, UASt-FLP/+

Video S3

control: w, UASt-trol RNAi/+; +/CyO

w; trol::GFP

Video S4

bab1>trol RNAi: w, UASt-trol RNAi/+;; bab1-Gal4/+

Immunohistochemistry

Adult flies were yeasted for 2 days before dissection in PBT (PBS + 0.1% Tween 20). Ovary stainings were performed at room temperature as described in [52]. Chemical dyes were added after antibody incubation. To visualise actin filaments samples were incubated 20 minutes in PBT + 1:20 Rhodamine-phalloidin. To detect DNA, samples were incubated for 10 minutes in PBT + Hoechst (Sigma, 5mg/ml; used 1:1000).

To stain third instar larval gonads, dissected gonads embedded in larval fat body were incubated in 5% formaldehyde in Ringer's medium for 20 minutes and then washed for 5, 10 and 45 minutes in 1% PBT (PBT + 1% BSA) [53]. Samples were blocked with 0.3% PBTB (0.3% Triton X-100 and 1% BSA in PBS) for one hour with gentle agitation and incubated with the primary antibody diluted in 0.3% PBTB overnight at 4°C with agitation. Next day, samples were washed three times in 0.3% PBTB and blocked with 0.3% PBTB supplemented with 5%

foetal bovine serum (FBS, Sigma) for 1 hour. After blocking, samples were incubated with the secondary antibodies in blocking solution for 2 hours. Samples were washed three times in 0.3% PBT and mounted in VECTASHIELD (Vector Laboratories).

Primary antibodies used were: Mouse monoclonal anti-Hts (Developmental Studies Hybridoma Bank, DSHB), 1:100; Mouse monoclonal anti-Lamin C (DSHB), 1:100; Rabbit anti-Vasa (a gift from R. Lehmann), 1:2000; Rat anti-*D*E-cadherin, DCAD2 (DSHB), 1:100; Mouse monoclonal anti-Engrailed, 4D9 (DSHB), 1:10; Goat anti-GFP, FITC-conjugated (Abcam, ab6662), 1:500; Rabbit anti-Nidogen [54], 1:100; Rabbit anti-Laminin β1 [55], 1:1000; Guinea pig anti-Hedgehog [56], 1:500; Guinea pig anti-Traffic Jam (a gift from D. Godt) [57], 1:5000. The anti-Perlecan antibody was raised by ProteoGenix SAS (France) following a protocol based on [25]. In short, a 2310bp cDNA coding for Domain V of the Perlecan protein was codon optimised for its expression in mammalian cells and ligated into an episomal expression vector. The vector was transfected into human 293-EBNA cells (Invitrogen) and serum-free medium was collected for protein purification. Antibodies were obtained after Ni-affinity purification followed by size-exclusion chromatography. Immunisation of rabbits and affinity-purification of antibodies followed standard protocols [58]. The affinity-purified antibody was used at a concentration of 1:2000. Antibody specificity was demonstrated by the lack of Perlecan staining in CpCs homozygous for a protein-null mutation in the *trol* gene and by the strong reduction in Perlecan levels upon *trol RNAi* knock-down (see main text). Secondary antibodies FITC, Cy2, Cy3 and Cy5 (Jackson Immuno Research Laboratories, Inc.) were used at 1:100.

Imaging of fixed samples

Images were acquired with a Leica SP5 confocal microscope, analysed utilising Imaris and ImageJ, and processed with Adobe Photoshop and Adobe Illustrator. 3-D images of fixed samples were taken with a 40x/1.3 NA or 63x/1.4 NA oil immersion objectives.

Transmission Electron Microscopy (TEM)

TEM samples were prepared following standard procedures. Briefly, ovaries were dissected in PBS + 0.1% Tween-20 and fixed for 2 hours at 4°C in 3% glutaraldehyde/l% paraformaldehyde

(vol./vol.) in 0.05 M cacodylate buffer (pH 7.4). After three 10 min. washes in cacodylate buffer 0.1 M at 4°C, ovaries were postfixed for 1 hour at 4°C in the dark (1% OsO_4, 1% $K_3Fe[CN]_6$ in water) and rinsed three times in distilled water at 4°C and stained for 2 hours at room temperature (RT) in darkness (0.5% uranyl acetate). Next, ovaries were rinsed in distilled water and dehydrated through an ethanol rising series (50%, 70%, 90% and 3x100%; 10 min. each) at RT. Ovaries were then infiltrated with Embed 812 resin (Electron Microscopy Sciences) as follows: EMbed 812/ethanol 100%. 1:2, 1:1 and 2:1 for 1 hour at RT each, and in EMbed 812 overnight at 4°C. The resin-embedded specimens were polymerised by incubation in fresh EMbed 812 during 48 hours at 60°C in flat plastic embedding molds. The inclusion blocks were cut in 50-70 nm thick sections with a DIATOME diamond-blade fixed on a Reichert Jung Ultramicrotome and mounted on copper grids. Sections were counterstained with 1% uranyl acetate in 50% ethanol for 1 min. and then stained with lead citrate for 5 min. in a CO_2-free atmosphere [59]. Sections were examined with a Zeiss EM902 electron microscope at 80Kv, and photographed at 50.000x magnification.

Targeted DamID (TaDa)

The Targeted DamID (TaDa) technique is a variation of DNA adenine methyltransferase identification (DamID). The TaDa approach assesses genome-wide protein binding *in vivo* in a cell type-specific manner but without the need for cell isolation or purification. In short, TaDa utilises the Gal4/UAS system to express a fusion of the Dam methylase and the RNA polymerase II core subunit RpII215 (Dam-Pol II) in specific cell types. Dam-Pol II in turn tags interacting chromatin by methylating adenines within GATC sequences. RNA Pol II occupancy can then be identified upon digestion of isolated genomic DNA with the methylation-sensitive DpnI enzyme. Subsequent sequencing of the digested DNA fragments allows the profiling of RNA Pol II occupancy in cells of interest [29].

Flies carrying the *UASt-LT3-Dam tub-Gal80^{ts}* or the *UASt-LT3-DamPolII tub-Gal80^{ts}* systems [29] were crossed to *en-Gal4*, *bab1-Gal4* or *tj-Gal4* and reared at 18°C. After hatching, adults were placed at 29°C for 24 hours to induce Dam-PolII or Dam expression. Genomic DNA was extracted from 150 dissected ovaries per replicate (Qiagen DNeasy kit, 69181) and methylated DNA processed and amplified as described [60]. Briefly, genomic DNA

was digested overnight with DpnI (NEB) (which cuts methylated GATC sequences) and adaptor sequences ligated to the cut DNA fragments. Following a subsequent digestion with DpnII (NEB) (which selectively cuts at unmethylated GATC sites), fragments with consecutive methylated GATCs were amplified via PCR using primers specific to the ligated adaptors using Advantage cDNA polymerase (Clontech).

DamID samples were prepared for next-generation sequencing as previously described [60]. Briefly, DNA was sonicated using a Bioruptor Plus (Diagenode) to an average fragment size of 300bp and DamID were adaptors removed through digestion with Sau3AI, before end-repair, A-tailing, Illumina adaptor ligation, and PCR amplification. 50bp single-end reads were obtained via a HiSeq 1500 (Illumina).

We processed and sequenced two biological replicates for the *tj-GAL4* driver, and one replicate each of the *en-Gal4* and *bab1-GAL4* drivers. Results are listed in Data S1.

DamID analysis

Illumina NGS reads were aligned back to the Dm6 reference genome and enrichment profiles calculated using damidseq_pipeline with default settings [61], and replicates were scaled and averaged. Pol II occupancy figures were generated using pyGenomeTracks [62, 63]. Pol II occupancy across gene bodies was determined using polii.gene.call [60] with genes considered to have significant Pol II occupancy at FDR<0.01.

QUANTIFICATION AND STATISTICAL ANALYSIS

Data Analysis

To quantify fluorescent signal in control and experimental samples images were captured using identical confocal settings. Z-sections were taken every 0.5 µm. Colour depth was set to 8-bit and configured so that most pixels were within the range of detection. Fluorescent intensities of the FITC, GFP or Cyanine markers used were quantified in the CpC and TF region of the niche by drawing small boxes. When appropriate, paired comparisons of cells and/or cell boundaries of the same germarium or larval gonad were done. Quantification was performed only in germaria lacking the muscle sheath. Image stacks were pre-processed using the standard background subtraction function of ImageJ. For quantifications, we utilised

the “Measurement points” tool of the IMARIS software and/or the “ROI measurement” tool from ImageJ.

Statistical Analysis

Experiments were performed with at least three biological replicas. Germaria were collected from at least 5 different adult females grown under equivalent environmental conditions. The average values ± standard deviations are represented. P-values were obtained using a Student’s t-test to determine values that were significantly different (*: P≤0.05, **: P≤0.005, ***: P≤0.0005). Numbers in Figures 3B-F, S2E and S3B, S3E and S3F refer to number of germaria analysed (n).

SUPPLEMENTAL VIDEOS

Video S1: *bab1>trol RNAi* germarium harbouring a displaced cluster of CpCs. Related to Figure 3. The video is a collection of confocal planes along the z axis of an experimental germarium grown at 25^{o}C and containing a cluster of Lamin C-positive CpCs detached from the base of the terminal filament. Lamin C (white) marks CpCs. DNA is shown in blue.

Video S2: Mosaic germarium harbouring *trol*$^{-}$ CpCs. Related to Figure 3. The video is a collection of confocal planes along the z axis of an experimental germarium containing several *trol*$^{-}$ CpCs, some displaced from the rosette located at the base of the terminal filament. Mutant cells are labelled by the loss of GFP staining (green). Lamin C (white) marks CpCs. Perlecan (red) and DNA (blue) are also shown. z1, z2, z4 and z5 correspond to displaced CpCs in different planes.

Video S3: Distribution of Perlecan and Perlecan::GFP in late third instar female larval gonads. Related to Figure 4. The first video is a collection of confocal planes along the z axis of a control gonad stained with anti-Engrailed to label TF cells and CpCs (white), anti-Traffic jam to mark CpCs and intermingled cells (red) and anti-Perlecan (green). The second video is a

collection of confocal planes along the z axis of a *trol::GFP* gonad stained with anti-Hts to label cell periferies (white) and anti-GFP (green) to mark Perlecan::GFP expression.

Video S4: *bab1>trol RNAi* germarium harbouring a displaced CpC. Related to Figure 4. The video is a collection of confocal planes along the z axis of an experimental germarium grown at 25ºC and containing a Lamin C-positive CpC displaced from the rosette located at the base of the terminal filament (arrow). Lamin C (white) marks CpCs. Perlecan (green) and DNA (blue) are also shown.

SUPPLEMENTAL DATASET

Data S1: Genes with significant Pol II occupancy in *en-Gal4* + *bab1-Gal4* cells and in *tj-Gal4* positive cells. Related to Figure 2 and STAR Methods.

REFERENCES

1. Ohlstein, B., Kai, T., Decotto, E., and Spradling, A. (2004). The stem cell niche: theme and variations. Curr Opin Cell Biol *16*, 693-699.

2. Schofield, R. (1978). The relationship between the spleen colony-forming cell and the haemopoietic stem cell. Blood cells *4*, 7-25.

3. Pearson, J., Lopez-Onieva, L., Rojas-Rios, P., and Gonzalez-Reyes, A. (2009). Recent advances in Drosophila stem cell biology. Int J Dev Biol *53*, 1329-1339.

4. Ahmed, M., and Ffrench-Constant, C. (2016). Extracellular Matrix Regulation of Stem Cell Behavior. Curr Stem Cell Rep *2*, 197-206.

5. Niklason, L.E. (2018). Understanding the Extracellular Matrix to Enhance Stem Cell-Based Tissue Regeneration. Cell Stem Cell *22*, 302-305.

6. Pearson, J., Zurita, F., Díaz-Torres, A., Díaz de la Loza, M., Franze, K., Martín-Bermudo, M., and González-Reyes, A. (2016). ECM-regulator timp is requiered for stem cell niche organization and cyst production in the Drosophila ovary. PLoS genetics *12*, e1005763. doi:1005710.1001371/journal.pgen.1005763.

7. Yui, S., Azzolin, L., Maimets, M., Pedersen, M.T., Fordham, R.P., Hansen, S.L., Larsen, H.L., Guiu, J., Alves, M.R.P., Rundsten, C.F., et al. (2018). YAP/TAZ-Dependent Reprogramming of Colonic Epithelium Links ECM Remodeling to Tissue Regeneration. Cell Stem Cell *22*, 35-49.e37.

8. Wang, X., and Page-McCaw, A. (2014). A matrix metalloproteinase mediates long-distance attenuation of stem cell proliferation. J Cell Biol *206*, 923-936.

9. Weaver, L.N., and Drummond-Barbosa, D. (2018). Maintenance of Proper Germline Stem Cell Number Requires Adipocyte Collagen in Adult Drosophila Females. Genetics *209*, 1155-1166.

10. O'Reilly, A.M., Lee, H.H., and Simon, M.A. (2008). Integrins control the positioning and proliferation of follicle stem cells in the Drosophila ovary. J Cell Biol *182*, 801-815.

11. Van De Bor, V., Zimniak, G., Papone, L., Cerezo, D., Malbouyres, M., Juan, T., Ruggiero, F., and Noselli, S. (2015). Companion Blood Cells Control Ovarian Stem Cell Niche Microenvironment and Homeostasis. Cell Rep *13*, 546-560.

12. Yurchenco, P.D. (2011). Basement membranes: cell scaffoldings and signaling platforms. Cold Spring Harb Perspect Biol *3*.

13. Farach-Carson, M.C., and Carson, D.D. (2007). Perlecan--a multifunctional extracellular proteoglycan scaffold. Glycobiology *17*, 897-905.

14. Grigorian, M., Liu, T., Banerjee, U., and Hartenstein, V. (2013). The proteoglycan Trol controls the architecture of the extracellular matrix and balances proliferation and differentiation of blood progenitors in the Drosophila lymph gland. Dev Biol *384*, 301-312.

15. Kamimura, K., Ueno, K., Nakagawa, J., Hamada, R., Saitoe, M., and Maeda, N. (2013). Perlecan regulates bidirectional Wnt signaling at the Drosophila neuromuscular junction. J Cell Biol *200*, 219-233.

16. Lindner, J.R., Hillman, P.R., Barrett, A.L., Jackson, M.C., Perry, T.L., Park, Y., and Datta, S. (2007). The Drosophila Perlecan gene trol regulates multiple signaling pathways in different developmental contexts. BMC Dev Biol *7*, 121.

17. Park, Y., Rangel, C., Reynolds, M.M., Caldwell, M.C., Johns, M., Nayak, M., Welsh, C.J., McDermott, S., and Datta, S. (2003). Drosophila perlecan

modulates FGF and hedgehog signals to activate neural stem cell division. Dev Biol *253*, 247-257.

18. Voigt, A., Pflanz, R., Schafer, U., and Jackle, H. (2002). Perlecan participates in proliferation activation of quiescent Drosophila neuroblasts. Dev Dyn *224*, 403-412.

19. Xie, T., and Spradling, A. (2000). A niche maintaining germ line stem cells in the Drosophila ovary. Science *290*, 328-330.

20. Panchal, T., Chen, X., Alchits, E., Oh, Y., Poon, J., Kouptsova, J., Laski, F.A., and Godt, D. (2017). Specification and spatial arrangement of cells in the germline stem cell niche of the Drosophila ovary depend on the Maf transcription factor Traffic jam. PLoS genetics *13*, e1006790.

21. Song, X., Zhu, C.H., Doan, C., and Xie, T. (2002). Germline stem cells anchored by adherens junctions in the Drosophila ovary niches. Science *296*, 1855-1857.

22. Medioni, C., and Noselli, S. (2005). Dynamics of the basement membrane in invasive epithelial clusters in Drosophila. Development *132*, 3069-3077.

23. Morin, X., Daneman, R., Zavortink, M., and Chia, W. (2001). A protein trap strategy to detect GFP-tagged proteins expressed from their endogenous loci in Drosophila. Proc Natl Acad Sci U S A *98*, 15050-15055.

24. Datta, S., and Kankel, D. (1992). l(1)trol and l(l)devl, Loci Affecting the Development of the Adult Central Nervous System in Drosophila melanogaster. Genetics *130*, 523-537.

25. Friedrich, M., Schneider, M., Timpl, R., and Baumgartner, S. (2000). Perlecan domain V ofDrosophila melanogasterSequence, recombinant analysis and tissue expression. Eur. J. Biochem. *267*, 3149-3159.

26. Schneider, M., Khalil, A.A., Poulton, J., Castillejo-Lopez, C., Egger-Adam, D., Wodarz, A., Deng, W.M., and Baumgartner, S. (2006). Perlecan and Dystroglycan act at the basal side of the Drosophila follicular epithelium to maintain epithelial organization. Development *133*, 3805-3815.

27. Gilboa, L., and Lehmann, R. (2004). How different is Venus from Mars? The genetics of germ-line stem cells in Drosophila females and males. Development *131*, 4895-4905.

28. Greenspan, L.J., de Cuevas, M., and Matunis, E. (2015). Genetics of gonadal stem cell renewal. Annu Rev Cell Dev Biol *31*, 291-315.

29. Southall, T.D., Gold, K.S., Egger, B., Davidson, C.M., Caygill, E.E., Marshall, O.J., and Brand, A.H. (2013). Cell-type-specific profiling of gene expression and chromatin binding without cell isolation: assaying RNA Pol II occupancy in neural stem cells. Dev Cell *26*, 101-112.

30. Li, M.A., Alls, J.D., Avancini, R.M., Koo, K., and Godt, D. (2003). The large Maf factor Traffic Jam controls gonad morphogenesis in *Drosophila*. Nat Cell Biol *5*, 994-1000.

31. Decotto, E., and Spradling, A.C. (2005). The Drosophila ovarian and testis stem cell niches: similar somatic stem cells and signals. Dev Cell *9*, 501-510.

32. Forbes, A., Lin, H., Ingham, P., and Spradling, A. (1996). hedgehog is required for the proliferation and specification of ovarian somatic follicle cells prior to egg chamber formation in Drosophila. Development *122*, 1125-1135.

33. Song, X., Wong, M.D., Kawase, E., Xi, R., Ding, B.C., McCarthy, J.J., and Xie, T. (2004). Bmp signals from niche cells directly repress transcription of a differentiation-promoting gene, bag of marbles, in germline stem cells in the Drosophila ovary. Development *131*, 1353-1364.

34. Xie, T., and Spradling, A. (1998). decapentaplegic is essential for the maintenance and division of germline stem cells in the Drosophila ovary. Cell *94*, 251-260.

35. Zhang, Y., and Kalderon, D. (2001). Hedgehog acts as a somatic stem cell factor in the Drosophila ovary. Nature *410*, 599-604.

36. Tazuke, S., Schulz, C., Gilboa, L., Fogarty, M., Mahowald, A., Guichet, A., Ephrussi, A., Wood, C., Lehmann, R., and Fuller, M. (2002). A germline-specific gap junction protein required for survival of differentiating early germ cells. Development *129*, 2529-2539.

37. Lopez-Onieva, L., Fernandez-Minan, A., and Gonzalez-Reyes, A. (2008). Jak/Stat signalling in niche support cells regulates dpp transcription to control germline stem cell maintenance in the Drosophila ovary. Development *135*, 533-540.

38. Dansereau, D.A., and Lasko, P. (2008). The development of germline stem cells in Drosophila. Meth. Mol. Biol. *450*, 3-26.

39. Yatsenko, A.S., and Shcherbata, H.R. (2018). Stereotypical architecture of the stem cell niche is spatiotemporally established by miR-125-dependent coordination of Notch and steroid signaling. Development *145*.

40. Sahut-Barnola, I., Godt, D., Laski, F., and Couderc, J.-L. (1995). Drosophila ovary morphogenesis: Analysis of terminal filament formation and identification of a gene required for this process. Dev. Biol. *170*, 127-135.

41. Jenkins, A.B., McCaffery, J.M., and Van Doren, M. (2003). Drosophila E-cadherin is essential for proper germ cell-soma interaction during gonad morphogenesis. Development *130*, 4417-4426.

42. Lai, C.M., Lin, K.Y., Kao, S.H., Chen, Y.N., Huang, F., and Hsu, H.J. (2017). Hedgehog signaling establishes precursors for germline stem cell niches by regulating cell adhesion. J Cell Biol *216*, 1439-1453.

43. Wang, X., and Page-McCaw, A. (2018). Wnt6 maintains anterior escort cells as an integral component of the germline stem cell niche. Development *145*.

44. Tepass, U., Gruszynski-DeFeo, E., Haag, T., Omatyar, L., Török, T., and Hartenstein, V. (1996). shotgun encodes Drosophila E-cadherin and is preferentially required during cell rearrangement in the neuroectoderm and other morphologically active epithelia. Genes & Dev. *10*, 672-685.

45. Sanchez-Sanchez, B.J., Urbano, J.M., Comber, K., Dragu, A., Wood, W., Stramer, B., and Martin-Bermudo, M.D. (2017). Drosophila Embryonic Hemocytes Produce Laminins to Strengthen Migratory Response. Cell Rep *21*, 1461-1470.

46. Pastor-Pareja, J.C., and Xu, T. (2011). Shaping cells and organs in Drosophila by opposing roles of fat body-secreted Collagen IV and perlecan. Dev Cell *21*, 245-256.

47. Watt, F.M., and Huck, W.T. (2013). Role of the extracellular matrix in regulating stem cell fate. Nat Rev Mol Cell Biol *14*, 467-473.

48. Andersen, D., and Horne-Badovinac, S. (2016). Influence of ovarian muscle contraction and oocyte growth on egg chamber elongation in Drosophila. Development *143*, 1375-1387.

49. Bolívar, J., Pearson, J., López-Onieva, L., and González-Reyes, A. (2006). Genetic dissection of a stem cell niche: the case of the *Drosophila* ovary. Dev Dyn *235*, 2969-2979.

50. Guo, Z., and Wang, Z. (2009). The glypican Dally is required in the niche for the maintenance of germline stem cells and short-range BMP signaling in the Drosophila ovary. Development *136*, 3627-3635.

51. Chou, T.-B., and Perrimon, N. (1992). Use of a yeast site-specific recombinase to produce female germline chimeras in Drosophila. Genetics *131*, 643-653.

52. Valencia-Exposito, A., Grosheva, I., Miguez, D.G., Gonzalez-Reyes, A., and Martin-Bermudo, M.D. (2016). Myosin light-chain phosphatase regulates basal actomyosin oscillations during morphogenesis. Nature communications *7*, 10746.

53. Maimon, I., and Gilboa, L. (2011). Dissection and staining of Drosophila larval ovaries. Journal of visualized experiments : JoVE.

54. Wolfstetter, G., Shirinian, M., Stute, C., Grabbe, C., Hummel, T., Baumgartner, S., Palmer, R., and Holz, A. (2009). Fusion of circular and longitudinal muscles in Drosophila is independent of the endoderm but further visceral muscle differentiation requires a close contact between mesoderm and endoderm. Mech. of Dev. *126*, 721-736.

55. Kumagai, C., Kadowaki, T., and Kitagawa, Y. (1997). Disulfide-bonding between *Drosophila* laminin β and γ chains is essential for α chain to form αβγ trimer. FEBS Lett *412*, 211-216.

56. Lobo-Pecellin, M., Marin-Menguiano, M., and Gonzalez-Reyes, A. (2019). mastermind regulates niche ageing independently of the Notch pathway in the Drosophila ovary. Open Biol *9*, 190127.

57. Gunawan, F., Arandjelovic, M., and Godt, D. (2013). The Maf factor Traffic jam both enables and inhibits collective cell migration in Drosophila oogenesis. Development *140*, 2808-2817.

58. Timpl, R. (1982). Antibodies to collagens and procollagens. Methods in Enzymology *82*, 831-838.

59. Reynolds, E.S. (1963). The use of lead citrate at high pH as an electron-opaque stain in electron microscopy. J Cell Biol *17*, 208-212.

60. Marshall, O.J., Southall, T.D., Cheetham, S.W., and Brand, A.H. (2016). Cell-type-specific profiling of protein-DNA interactions without cell isolation using targeted DamID with next-generation sequencing. Nat Protoc *11*, 1586-1598.

61. Marshall, O.J., and Brand, A.H. (2015). damidseq_pipeline: an automated pipeline for processing DamID sequencing datasets. Bioinformatics *31*, 3371-3373.

62. Ramirez, F., Bhardwaj, V., Arrigoni, L., Lam, K.C., Gruning, B.A., Villaveces, J., Habermann, B., Akhtar, A., and Manke, T. (2018). High-resolution TADs reveal DNA sequences underlying genome organization in flies. Nature communications *9*, 189.

63. López-Delisle, L., Rabani, L., J, W., Bhardwaj, V., Backofen, R., Grüning, B., Ramírez, F., and Manke, T. (2020). pyGenomeTracks: reproducible plots for multivariate genomic data sets. Bioinformatics *Aug 3:btaa692.*

KEY RESOURCES TABLE

REAGENT OR RESOURCE	SOURCE	IDENTIFIER
Antibodies		
mouse anti-Hts	Developmental Studies Hybridoma Bank	Cat# 1B1
mouse anti-Lamin C	Developmental Studies Hybridoma Bank	Cat# LC28.26
rabbit anti-Vasa	Prof. Ruth Lehmann	N/A
rat anti-*D*E-cadherin	Developmental Studies Hybridoma Bank	Cat# DCAD2
mouse anti-Engrailed	Developmental Studies Hybridoma Bank	Cat# 4D9
goat anti-GFP, FITC-conjugated	Abcam	Cat# ab6662
rabbit anti-Nidogen	[54]	N/A
rabbit anti-Laminin β1	[55]	N/A
guinea pig anti-Hedgehog	[56]	N/A
guinea pig anti-Traffic jam	[57]	N/A
rabbit anti-Perlecan	This work	N/A
Chemicals		
VECTASHIELD	Vector Laboratories	Cat# H1000; RRID:AB_2336789
PBS tablets	Sigma-Aldrich	Cat# P4417
Tween 20	Sigma-Aldrich	Cat# P9416
Rhodamine-phalloidin	Biotium	Cat# BT-00027
BSA	Sigma-Aldrich	Cat# 05470
FBS	Sigma-Aldrich	Cat# F2442
Triton x-100	Sigma-Aldrich	Cat# T8787
Glutaraldehyde	Sigma-Aldrich	Cat# G5882

EMbed 812	Electron Microscopy Sciences	Cat# 14120
Targeted DamID	[60]	N/A
Experimental Models: Organisms/Strains		
y w	Laboratory stock	RRID:BDSC_1495
trol^{null}	[18]	N/A
shg^{1}	[44]	N/A
UASt-trol RNAi	VDRC	22642
UASt-sh:GFP RNAi	VDRC	313432
en-Gal4	[50]	RRID:BDSC_30564
bab1-Gal4	[49]	N/A
tj-Gal4	[50]	N/A
UASt-LT3-Dam, UASt-LT3-Dam PolII	[29]	N/A
vkg::GFP	[22, 23]	N/A
trol::GFP	[23]	N/A
tub-Gal80^{ts}	BDSC	RRID:BDSC_7108
y w, hs-flp12 pUbi-nls GFP FRT-101	Laboratory stock	N/A
UASt-FLP	Laboratory stock	N/A
Software and Algorithms		
Fiji	Open Source	https://fiji.sc/
Imaris	Oxford Instruments	https://imaris.oxinst.com/
Deposited Data		
Raw sequencing data	This study	GEO accession number: GSE164866

Amended Figure 1

Click here to access/download;Figure;Fig 1_ECM components-7.tif

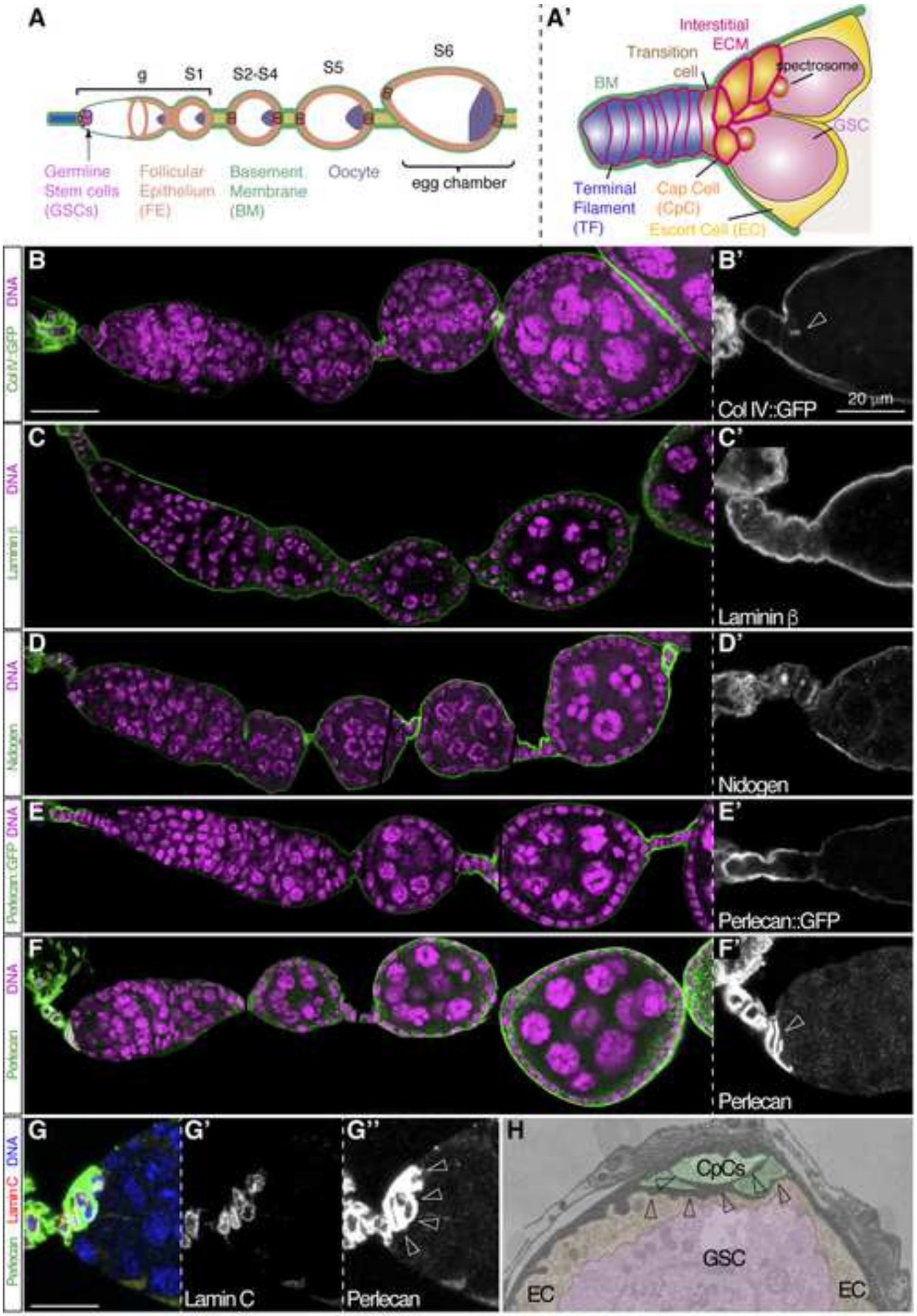

Amended Figure 2

Click here to access/download;Figure;Fig 2 TaDa-5 Owen5.tif

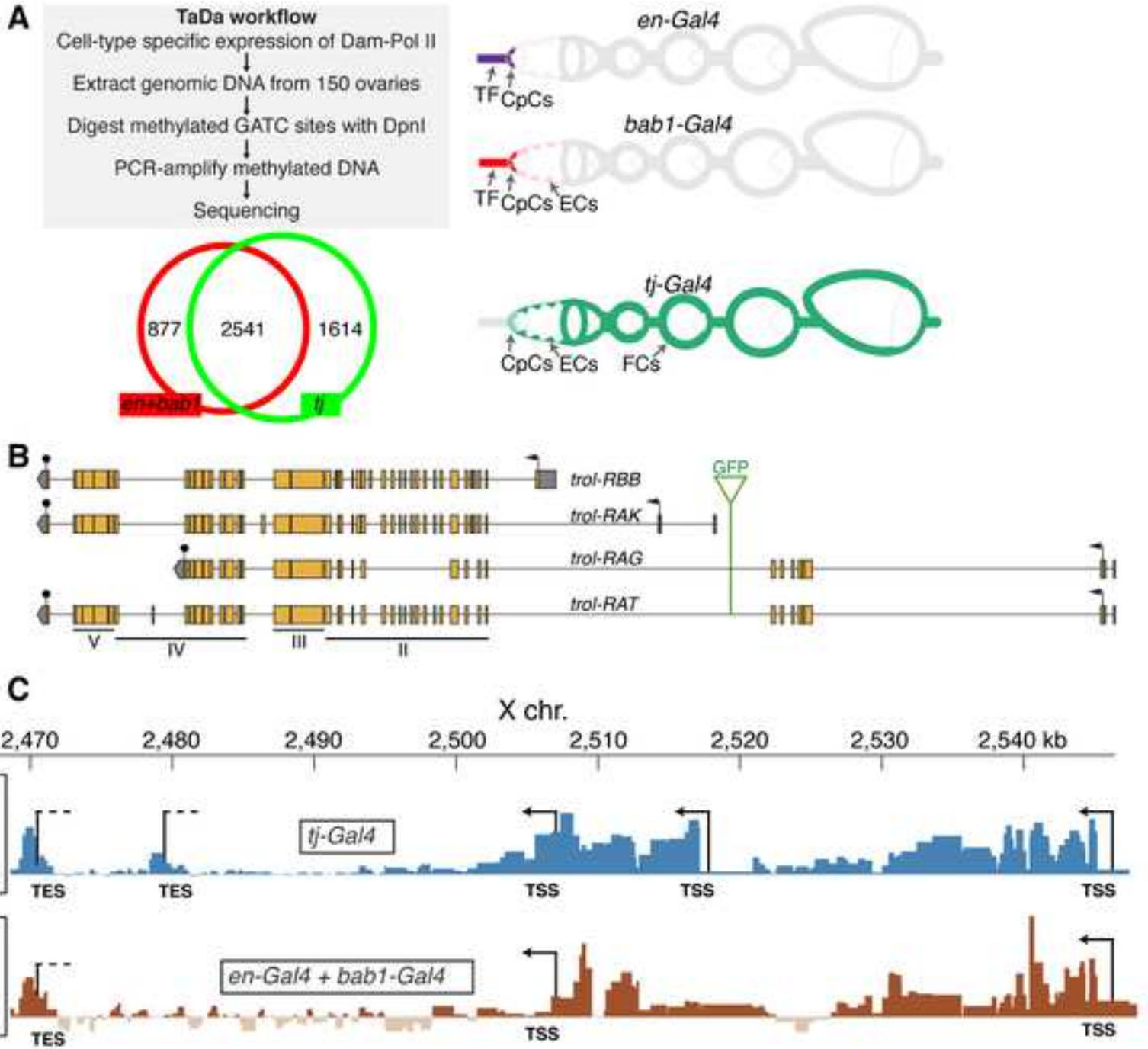

Amended Figure 3

Click here to access/download;Figure;Fig 3 CpC-8-CB 2nd subm-4.tif

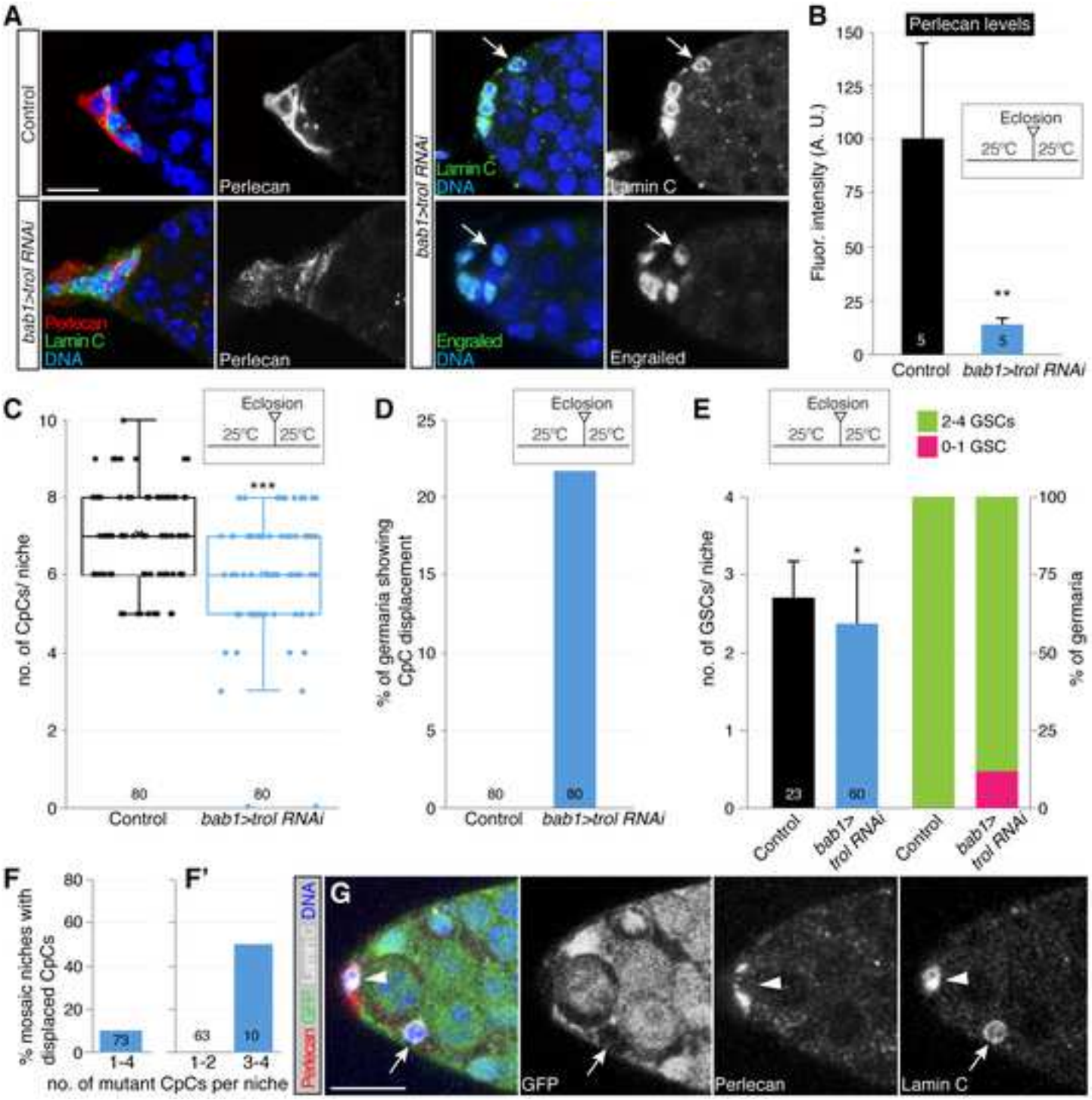

Amended Figure 4

Click here to access/download;Figure;Fig 4 Gonads-CB-4-FINAL subm.tif

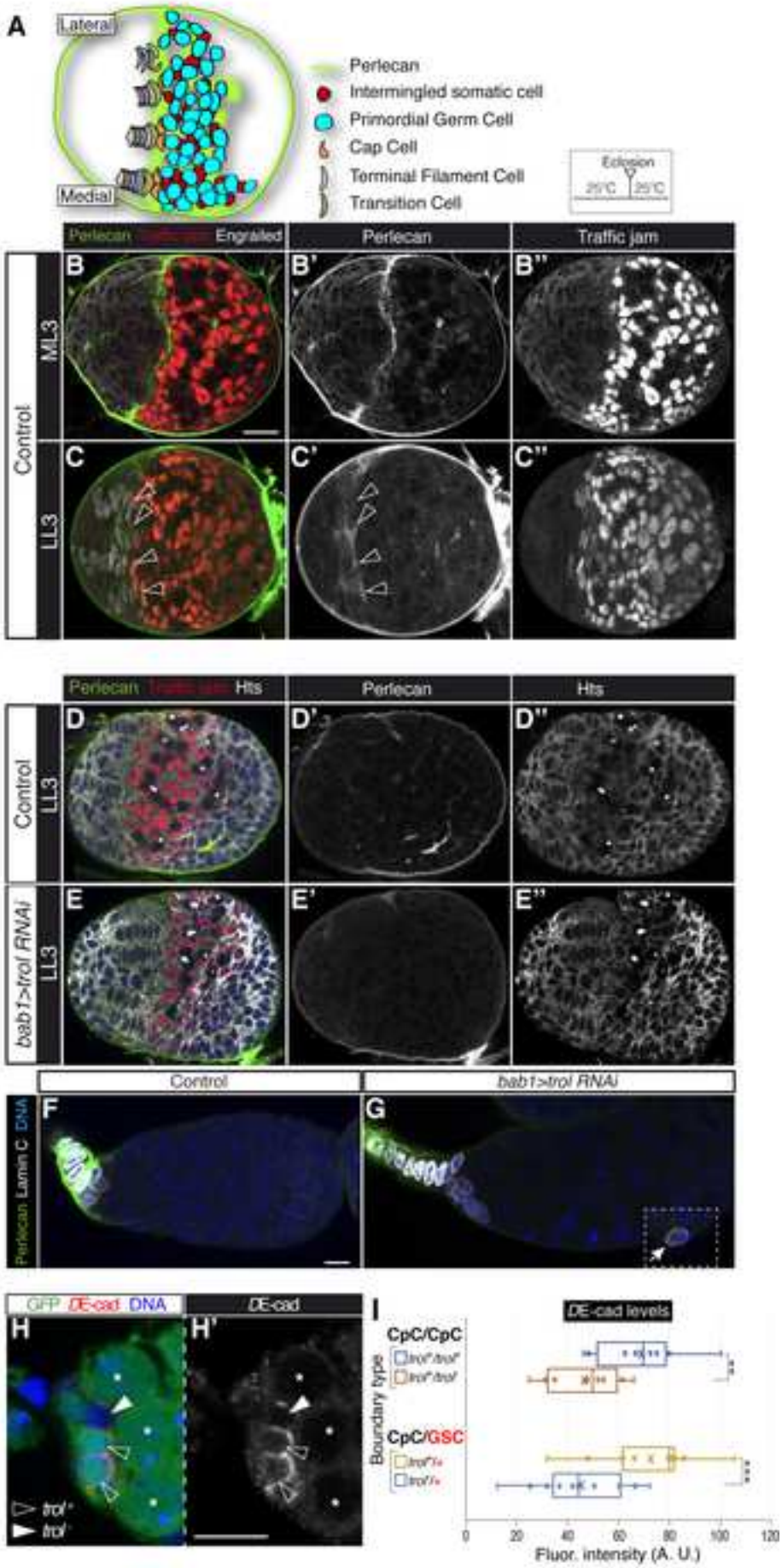

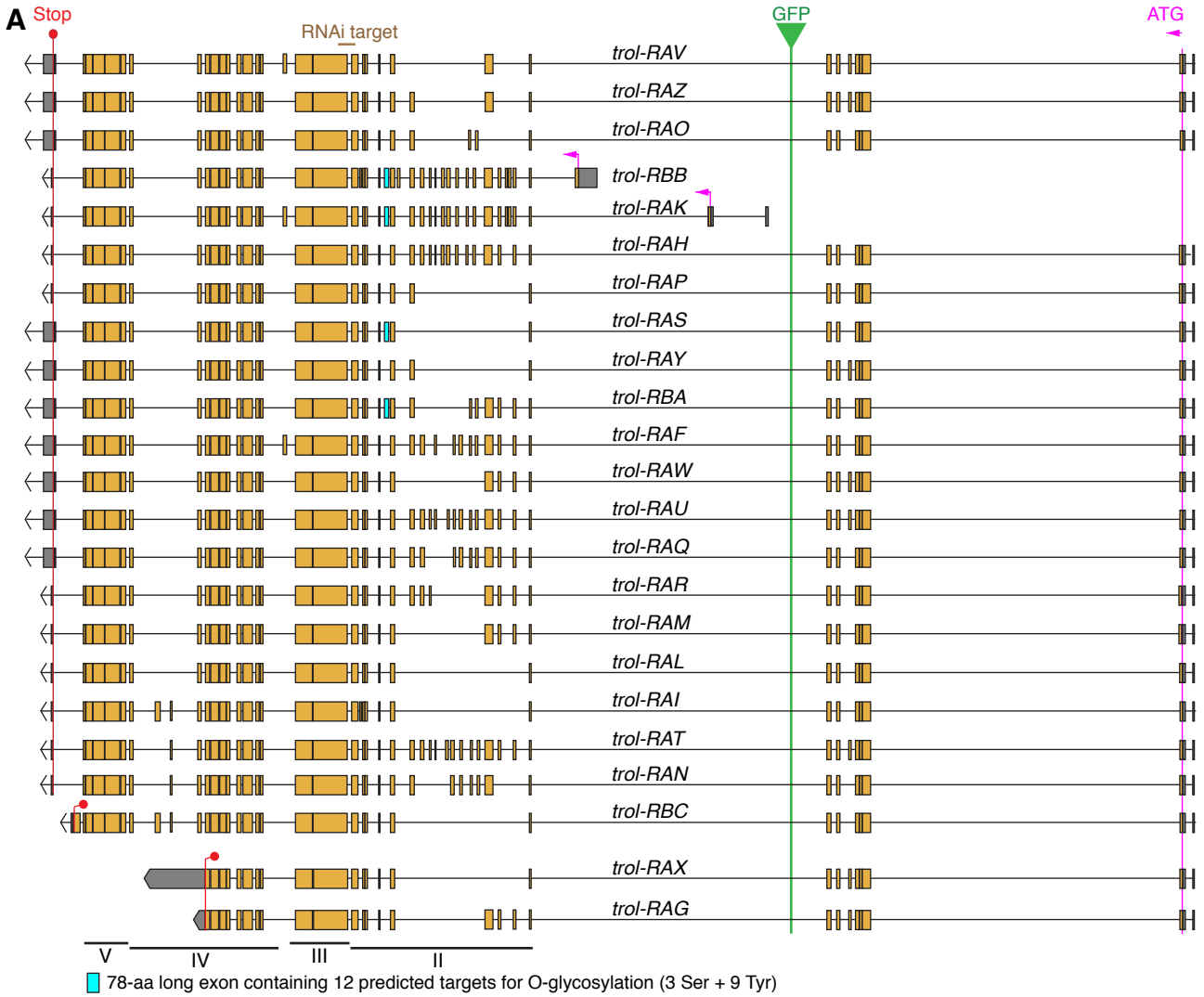
A
Stop
RNAi target
GFP
ATG
trol-RAV
trol-RAZ
trol-RAO
trol-RBB
trol-RAK
trol-RAH
trol-RAP
trol-RAS
trol-RAY
trol-RBA
trol-RAF
trol-RAW
trol-RAU
trol-RAQ
trol-RAR
trol-RAM
trol-RAL
trol-RAI
trol-RAT
trol-RAN
trol-RBC
trol-RAX
trol-RAG
V
IV
III
II
78-aa long exon containing 12 predicted targets for O-glycosylation (3 Ser + 9 Tyr)

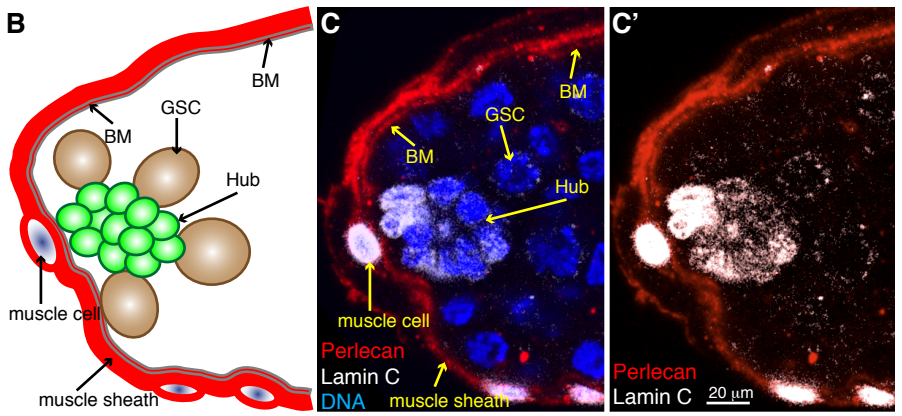
B
BM
GSC
BM
Hub
muscle cell
muscle sheath
C
BM
GSC
BM
Hub
muscle cell
Perlecan
Lamin C
DNA
muscle sheath
C'
Perlecan
Lamin C
20 µm

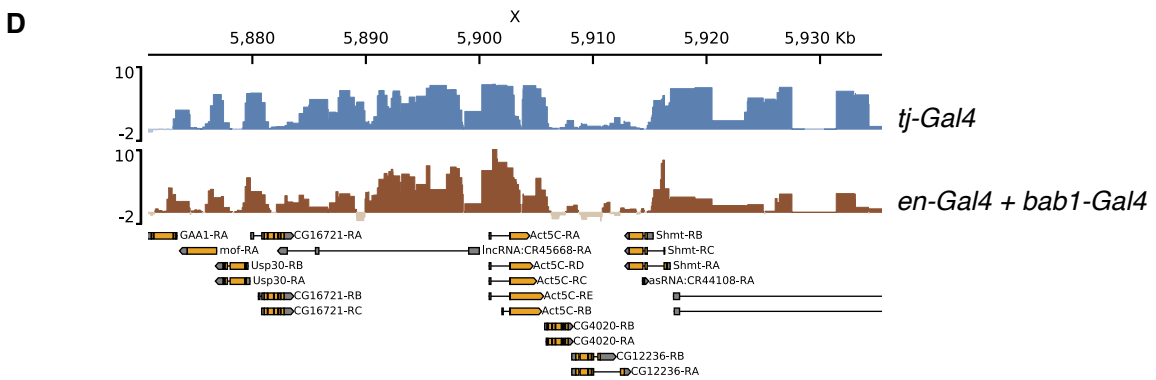
D
X
5,880
5,890
5,900
5,910
5,920
5,930 Kb
10
-2
tj-Gal4
en-Gal4 + bab1-Gal4
GAA1-RA
CG16721-RA
mof-RA
Usp30-RB
Usp30-RA
CG16721-RB
CG16721-RC
lncRNA:CR45668-RA
Act5C-RA
Act5C-RD
Act5C-RC
Act5C-RE
Act5C-RB
CG4020-RB
CG4020-RA
CG12236-RB
CG12236-RA
Shmt-RB
Shmt-RC
Shmt-RA
asRNA:CR44108-RA

Figure S1: Organisation of the *trol* gene. Perlecan accumulation in the male GSC niche. Transcription of the *Actin 5c (Act5c)* gene in different somatic cell types of the adult ovary. Related to Figures 1 and 2. (A) According to JBrowse (FlyBase2020_04), the *trol* gene can give rise to 23 different predicted isoforms. The ATGs corresponding to the long, intermediate and short versions, the STOP codons, the target sequence for the *trol RNAi* construct and the insertion point of the GFP exon are shown for all isoforms. Only the large isoforms are expected to incorporate GFP. The Perlecan antibody used in this study was raised against domain V of the protein. *Drosophila trol* lacks Domain I of the human orthologue gene. Exon in light blue is specific for only four isoforms and it is predicted to be O-glycosylated in 12 out of 78 residues. The RNAi target is shown in light brown. All isoforms should be targets of the interference construct. **(B)** Schematic representation of the *Drosophila* testis GSC niche. The anterior tip is home to the hub and a number of male GSCs attached to the hub cells. Each GSC is flanked by two somatic stem cells (cyst stem cells; not shown). The niche is surrounded by a basement membrane (BM) and an external muscle sheath. **(C)** Confocal image showing the tip of a *Drosophila* testis. Hub cells accumulate Lamin C (white) in a similar manner to CpCs. However, Perlecan (red) is not detected in the hub, even though it accumulates in the BM and the muscle sheath. Muscle cells also express nuclear Lamin C. DNA is shown in blue (Hoechst staining). **(D)** Cell-type-specific profiling of *Act5c* expression in TF cells, CpCs and ECs (*en-Gal4 + bab1-Gal4*) or in most of the somatic cells of the adult ovary (*tj-Gal4*) using the TaDa technique. Scale bars represent log2 ratio change between Dam-Pol II and Dam (reference) samples. The data are scaled so that the Pol II occupancy between the two different groups of cell types should be equivalent. Scale bar= 20µm.

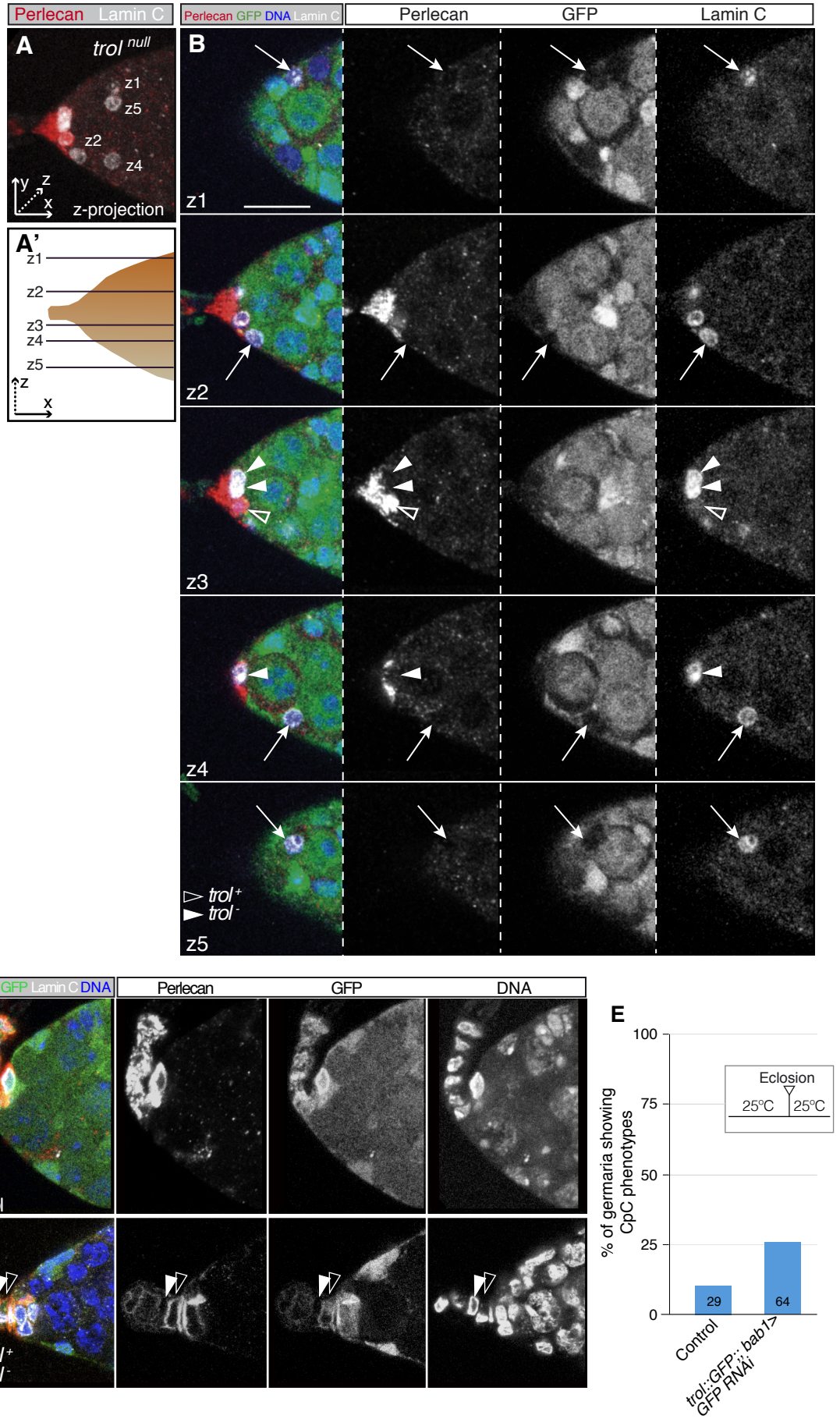
Perlecan Lamin C
A
trol null
z1
z5
z2
z4
y z
x
z-projection
A'
z1
z2
z3
z4
z5
z
x
Perlecan GFP DNA Lamin C
Perlecan
GFP
Lamin C
B
z1
z2
z3
z4
trol+
trol-
z5
Perlecan GFP Lamin C DNA
Perlecan
GFP
DNA
C
Control
D
trol+
trol-
E
% of germaria showing CpC phenotypes
100
75
50
25
0
Eclosion
25°C
25°C
29
64
Control
trol::GFP; bab1> GFP RNAi

Figure S2: Loss of *trol* activity induces cap cell displacement. Related to Figure 3. (A) Z-projection (top view) of a mosaic germarium containing several *trol* mutant CpCs. At least four of the *trol*$^{-}$ cells are not associated with the CpC rosette found at the base of the terminal filament. **(A')** Representation showing the different z-planes used in this analysis (lateral view). **(B)** Individual optical sections displaying the spatial arrangement of the mutant cells with respect to the anterior CpC rosette. CpCs are labelled with Lamin C. *trol* mutant cells are marked by the lack of GFP and Perlecan staining. Plane z3 shows a *trol*$^{+}$ CpC with high Perlecan levels. Its Lamin-C staining can be observed better in plane z2. **(C)** Z-sections of a control and **(D)** a mosaic germarium containing a *trol*$^{-}$ TF cell stained to visualise Perlecan, GFP, Lamin C and DNA. The mutant TF cell (GFP^{-}; solid arrowhead) shows a noticeable reduction in Perlecan levels. **(E)** Quantification of the number of abnormal niches containing displaced CpCs in control and in experimental (*trol::GFP;; bab1>GFP RNAi*) germaria grown at 25^{o}C. Numbers in bars refer to number of germaria analysed. Arrows: displaced *trol*$^{-}$ CpCs; empty arrowheads: control CpCs in the rosette; solid arrowheads: mutant CpCs in the rosette. (A, B) Clones were induced using the *bab1-Gal4/UASt-flp* system. (C) To increase the occurrence of mitotic recombination, in addition to inducing *flp* expression with the *bab1-Gal4/UASt-flp* system, flies of the appropriate genotype were subjected to heat-shock to express *flp* from the *hs-flp* construct (see STAR METHODS in the main text). Scale bar = 20µm.

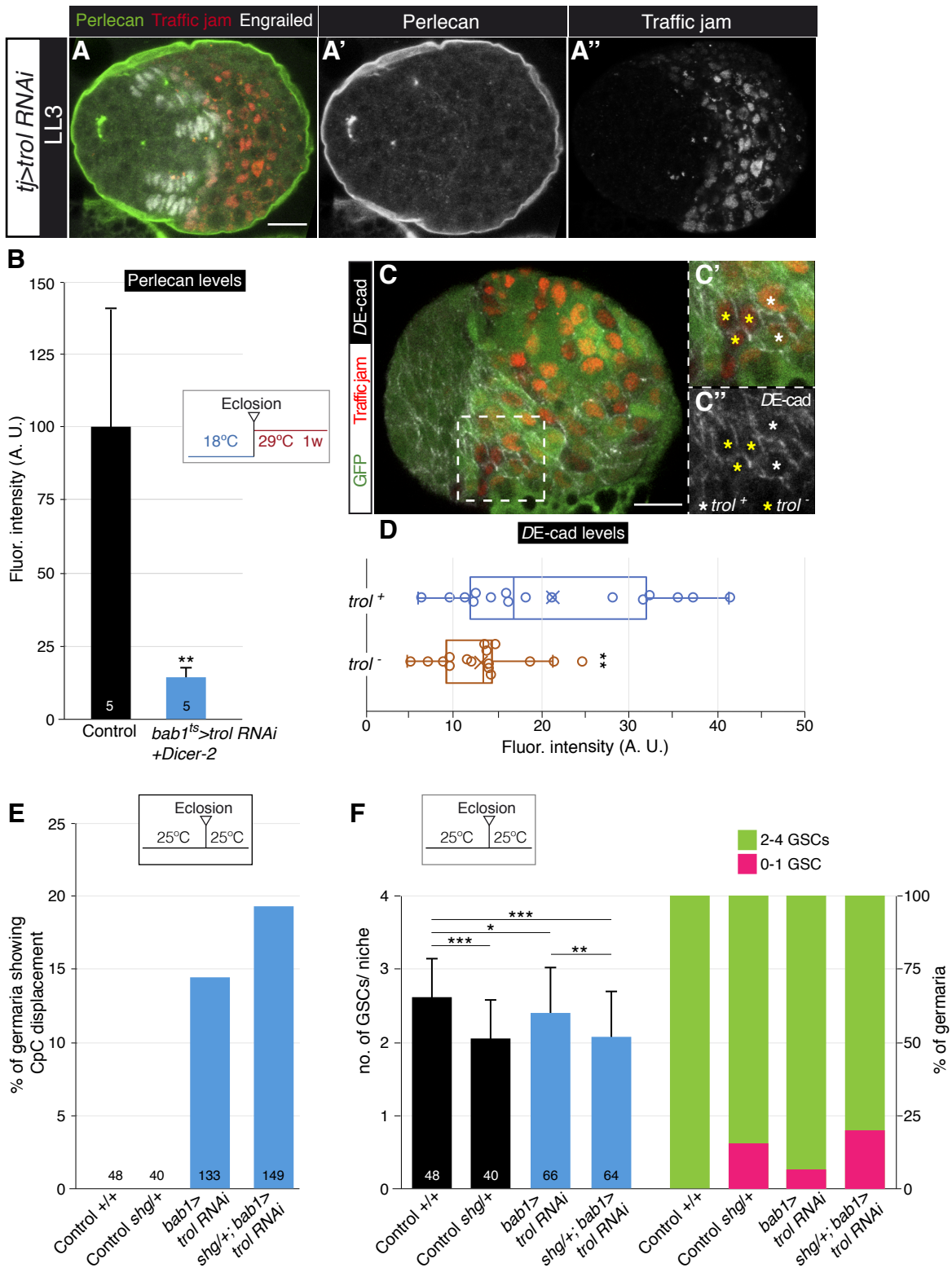
Perlecan Traffic jam Engrailed
Perlecan
Traffic jam
tj>trol RNAi
LL3
A
A'
A''
B
Perlecan levels
Fluor. intensity (A. U.)
Eclosion
18°C
29°C 1w
Control
bab1ts>trol RNAi
+Dicer-2
C
C'
C''
DE-cad
Traffic jam
GFP
trol +
trol -
D
DE-cad levels
Fluor. intensity (A. U.)
E
Eclosion
25°C 25°C
% of germaria showing CpC displacement
Control +/+
Control shg/+
bab1> trol RNAi
shg/+; bab1> trol RNAi
F
2-4 GSCs
0-1 GSC
no. of GSCs/ niche
% of germaria

Figure S3: Low Perlecan levels in *tj>trol RNAi* gonads. Quantification of Perlecan levels in *bab1^{ts}>trol RNAi+dicer* niches. Quantification of *D*E-cadherin levels in mosaic gonads. Genetic interaction between *shotgun* and *trol* in adult niches. Related to Figure 4. (A) Z-projection of a *tj>trol RNAi* LL3 gonad stained to visualise Perlecan, Traffic jam and Engrailed (to label TF cells). As an indication of the effectiveness of the *trol* RNAi tool, notice the strong reduction in Perlecan levels at the base of the TFs and in the PGC/ISC area. This experimental gonad corresponds to the control shown in Figure 4C. **(B)** Quantification of anti-Perlecan immunofluorescence signal in control and *bab1^{ts}>trol RNAi + Dicer-2* germaria grown at 18^{o}C and kept for 1 week at 29^{o}C upon eclosion. **(C)** Z-projection of a mosaic LL3 gonad stained to visualise Traffic jam, GFP and *D*E-cadherin. In this particular example, three mutant Tj-positive cells at the anterior limit of the germline cluster (considered to be prospective CpCs; yellow asterisks) are compared to neighbour control cells (white asterisks). **(D)** Quantification of *D*E-cadherin levels at *trol^{+}*/*trol^{+}* or *trol^{-}*/*trol^{-}* cell boundaries was performed on CpC or TF cells of LL3 gonads. *trol^{-}* cells localise significantly lower *D*E-cadherin amounts at their surfaces than *trol^{+}* cells. To allow for paired comparisons, measurements were taken from neighbouring control and experimental cells. P values of two-tailed, paired t-tests considered statistically significant between control and experimental samples are indicated (**: P≤0.005). The mean (cross) and median (line across box) for each of the samples are shown. We quantified 16 *trol^{+}* and 16 *trol^{-}* CpC or TF cell boundaries from 9 gonads. Clones were induced using the *hs-flp/FRT* system. **(E)** Percentage of control and experimental germaria showing displaced CpCs. **(F)** Quantification of the number of GSCs per niche and distribution of germaria containing 0-1 or 2-4 GSCs in control and experimental germaria. P values of two-tailed, unpaired t-tests considered statistically significant between control and experimental samples are indicated (*: P≤0.05, **: P≤0.005, ***: P≤0.0005). Numbers in bars refer to number of germaria analysed. Scale bars = 10μm.

Click here to access/download

Supplemental Videos and Spreadsheets

Data S1.xlsx

Video S1

Click here to access/download

Supplemental Videos and Spreadsheets

Video S2 CpC displ.avi

Click here to access/download

Supplemental Videos and Spreadsheets

Video S4 CpC displ_letters_arrow1.avi